Materials Today: Proceedings xxx (xxxx) 1–11

Contents lists available at ScienceDirect

Materials Today: Proceedings

journal homepage: www.elsevier.com

Structural, thermal and spectroscopic properties of Er_2O_3-doped oxyfluoro tellurophosphate glasses

B. Kiran Kumar [a, b], P. Reddi Babu [a], Virgílio de Carvalho dos Anjos [c], B. Deva Prasad Raju [a, *]

[a] Department of Physics, Sri Venkateswara University, Tirupati, 517 502, India
[b] Department of Physics, Government Degree College, Rayachoty-516 269, India
[c] Physics Department, Universidade Federal de Juiz de Fora, Campus Universitário, SN - Juiz de Fora - MG Zip, 36036-330, Brazil

ARTICLE INFO

Keywords:
Oxyfluoro tellurophosphate glasses
Er^{3+} ions
J-O analysis
Photoluminescence
Laser emission devices
Optical amplifiers

ABSTRACT

Employing the melt quench method, the oxyfluoro tellurophosphate glasses (PTBMEr), doped with varying erbium concentrations, were prepared . Their physical, structural, optical, and luminescent characteristics were investigated using XRD, EDX, FTIR, absorption and Photoluminescence studies . The amorphous nature and elemental composition were identified using the XRD and EDX spectra. The J-O parameters and radiative parameters, including energy gap (ΔE), branching ratio (β_R), radiative lifetime (τ_{rad}), and radiative transition probability (A_R), were established for different excited levels of erbium in PTBMEr glass matrices. The visible emission spectra were acquired through excitation at a wavelength of 377 nm, resulting in a highly pronounced emission band at 544 nm, corresponding to the transition $^4S_{3/2} \rightarrow {}^4I_{15/2}$. The NIR emission spectra obtained through excitation at 980 nm showed a prominent broad emission band at 1534 nm pertaining to the transition $^4I_{13/2} \rightarrow {}^4I_{15/2}$. Within the set of prepared samples, the PTBMEr05 sample exhibits highest stimulated emission cross section of 0.75×10^{-20} cm^2 for the transition $^4S_{3/2} \rightarrow {}^4I_{15/2.}$ It also exbited superior parameters for the transition $^4S_{3/2} \rightarrow {}^4I_{15/2}$ including a stimulated emission crosssection of 1.19×10^{-20} cm^2, gain bandwidth of 64.87×10^{-25} cm^3, and optical gain of 53.41×10^{-24} cm^2s. Experimental lifetime values for the excited level $^4I_{13/2}$ of erbium in PTBMEr glasses were calculated and found to decrease with concentration due to non-radiative mechanisms and concentration quenching. These results reflect that PTBMEr05 glass is best suited for green laser emission devices and optical fiber communication windows.

1. Introduction

Compact lasers possessing spectral ranges of operation in the near-infrared (up to 2 nm) and mid-infrared (2–5 nm) are useful for new-age medical technologies, eye-safe light detection, and optical communication applications. Within the domain of material engineering and infrared photonics, various systems, ranging from luminescent materials [1,2] to fiber-based sources [3] and optical devices, are influenced by these factors [4]. Trivalent Er^{3+} is considered a highly suitable option for diode-pumped lasers that emit radiation in the near-infrared (1500 nm) and mid-infrared (2700 nm) ranges because of the close proximity of $^4I_{13/2}$ and $^4I_{15/2}$ energy levels. In order to meet the needs of increasingly sophisticated optical data-transmission services, wavelength division multiplexing (WDM) systems need to be able to transmit more data. It is crucial to achieve broad-spectrum optical amplification that surpasses the conventional capabilities of erbium-doped fiber amplifiers (EDFA) within their operational window in order to optimize the utilization of silica-based optical fibers' low-loss spectrum (1300–1700 nm). The utility of broadband and/or tunable laser sources functioning in the mid-infrared region (2–5 nm) for industrial and atmospheric applications, on the other hand, creates a vital requirement. In glasses composed of inorganic materials with lower phonon energies, the rates of non-radiative multiphonon relaxation are frequently diminished. For active fiber and mid-infrared emission applications, the lowered phonon energy and improved transparency of these glasses are substantial benefits. Historically, practical implementations of mid-infrared luminescence were limited to low-phonon non-oxide systems, such as chalcogenide and fluoride, in addition to oxide systems including tellurite, germanate, and bismuthate glasses. Fluoride fibers are still limited in their application due to their poor chemical and mechanical stability. It is widely accepted that mixed oxyfluoride glasses can be a practical substitute for oxide and fluoride glasses in applications involving mid-infrared fibers. This is attributed to their ability to amalgamate the excellent thermal stability and mechanical properties and thermal

* Corresponding author.
E-mail address: drdevaprasadraju@gmail.com (B. Deva Prasad Raju).

https://doi.org/10.1016/j.matpr.2024.03.051
Received 5 February 2024; Received in revised form 19 March 2024; Accepted 21 March 2024
2214-7853/

Fig. 1. The photograph of various concentrations of PTBMEr glasses.

Table 1
Physical features of PTBMEr glasses.

Physical properties	PTBMEr05	PTBMEr10	PTBMEr15	PTBMEr20
Density (g / cm^3)	3.2182	3.2340	3.2850	3.3104
Thickness (cm)	0.39	0.40	0.39	0.38
Refractive index (n)	1.612	1.615	1.616	1.618
Dielectric constant (ϵ)	2.586	2.598	2.611	2.617
Concentration N (mol/ltr)	0.1139	0.2270	0.343	0.4570
Concentration N (ions / c.c × 10^{20})	0.686	1.367	2.066	2.752
Reflection loss (%)	5.433	5.489	5.546	5.569
Molar volume V_m (cm^3 / mol)	43.8982	43.8182	43.739	43.5575
Polaron Radius R_p (A^0)	9.84	7.82	6.81	6.19
Inter Ionic distance R_i (A^0)	24.42	19.41	16.91	15.37
Field strength F ($\times 10^{-14}$ cm^{-2})	3.097	4.906	6.469	7.830
Molar Refractivity (cm^{-3})	15.260	15.292	15.284	15.261
Electronic Polarizability ($\times 10^{-24}$ cm^3)	6.04	6.06	6.058	6.048

stability of oxide glasses with the enhanced radiation luminescent properties characteristic of fluoride glasses. Oxide glasses are enhanced by fluoride modifiers in order to enhance radiative transition contributions and result in significant increases in rare earth ion spectroscopic parameters, including luminescence lifetimes, stimulated emission cross section, and quantum efficiency.

The synthesis of glass compositions with elevated phosphorus content in recent years has garnered significant interest in phosphate glasses. Their attention is driven by the stability exhibited in chemical reactions. Phosphate glasses were successfully applied to several fields of materials due to their improved chemical stability [5–8]. There are several fields of science involved in this, such as photonic materials, biomedical materials, solid-state lasers using rare-earth ions, fast ionic conductors, and hermetic seals [9]. Apart from their potential as suitable options for low-melting glasses, phosphate glasses are also attracting interest because of their properties. Their glass transition temperature is low, their thermal expansion coefficient is appropriate, and their viscosity is low [10]. The interaction of three adjacent PO_4 tetrahedra, which are in vitrous P_2O_5, generates a three-dimensional network. Network depolymerization occurs when oxide is introduced to P_2O_5 resulting in the formation of non-bridging oxygen and the fragmentation of P-O linkages. Consequently, the modifying cations have the ability to establish ionic cross-links between the non-bridging oxygen atoms of two phosphate chains. This process enhances the binding between these molecules, leading to increased chemical endurance and mechanical strength in the glasses.

The primary aim of this study is to synthesize glasses and acquire a comprehensive understanding of the physical, structural, and spectroscopic characteristics of P_2O_5 + TeO_2 + $BaCO_3$ + MgF_2 doped with Er^{3+} ions, with the specific purpose of developing them for mid-infrared applications.

2. Experimental techniques

2.1. Sample preparation

(60-x) P_2O_5-10TeO_2-15$BaCO_3$-15MgF_2-xEr_2O_3 is the composition of the glass under investigation. Where x represents the molar percentage of Er_2O_3 and takes on values of 0.5, 1, 1.5, and 2% mol. The resulting structures are frequently referred to as PTBMEr05, PTBMEr10, PTBMEr15, and PTBMEr20, respectively. The glasses were prepared via the melt quenching process. According to the aforementioned compositions, constituent chemicals were precisely quantified for a batch of 20 g. In turn, the specimens were placed into the agate mortar and thoroughly homogenized until a uniform mixture was achieved. Then it was shifted into a crucible made of alumina and placed inside a furnace, where it underwent a heating procedure for a duration of 2 hours at a temperature of 1100 ˚C. A molten liquid that was produced by the process of heating was poured over a heated brass plate. The brass plate was inserted into a distinct furnace that had been heated to a temperature of 375 ˚C through the process of annealing. The plate was then maintained at the same temperature for 12 hours. The purpose of this action was to mitigate strain and thermal stress. Following this, the resulting glass samples underwent cooling until they reached ambient temperature. Subsequently, the samples underwent a rigorous polishing process in order to attain transparency and guarantee their preparedness for the subsequent optical characterization procedure. The photograph depicting the PTBMEr glasses that were obtained is presented in Fig. 1.

2.2. Characterizations

Utilizing monobromonapthalene as a contact liquid, the Abbe refractometer was employed to ascertain the refractive index at a wavelength of 589 nm. The capture of X-ray diffraction profiles was carried out utilizing the RIGAKU X-ray diffractometer, which encompassed a 2θ interval ranging from 10˚ to 80˚. The FTIR spectra of the synthesized glasses were obtained using the BRUKER ALPHA-II FTIR spectrometer, which has a spectral resolution of 2 cm^{-1}. The spectra were obtained over a range of 500–4000 cm^{-1}. The Oxford INCA FETX3 apparatus was deployed for the purpose of accomplishing energy dispersive X-ray (EDX) analysis. The UV–Vis-NIR spectrometer (JASCO model V-570) and the FLS-980 FluoroLog-3 spectrometer were employed to measure optical absorption spectra and photoluminescence spectra, respectively.

3. Results and discussions

3.1. Physical properties

The computation of physical parameters like average molecular weight, density, rare earth ion concentration, electronic polarizability, inter-ionic distance, dielectric constant, reflection loss, field strength, polaron radius, molar volume, and molar refractivity was done by employing the formulae documented in the existing literature [11,12]. The obtained values are outlined in Table 1. The rise in density is marked by the substitution of low molecular weight P_2O_5 with Er_2O_3. A reciprocal relationship can be seen between polaron radius and field strength, in correlation with the literature [13,14].

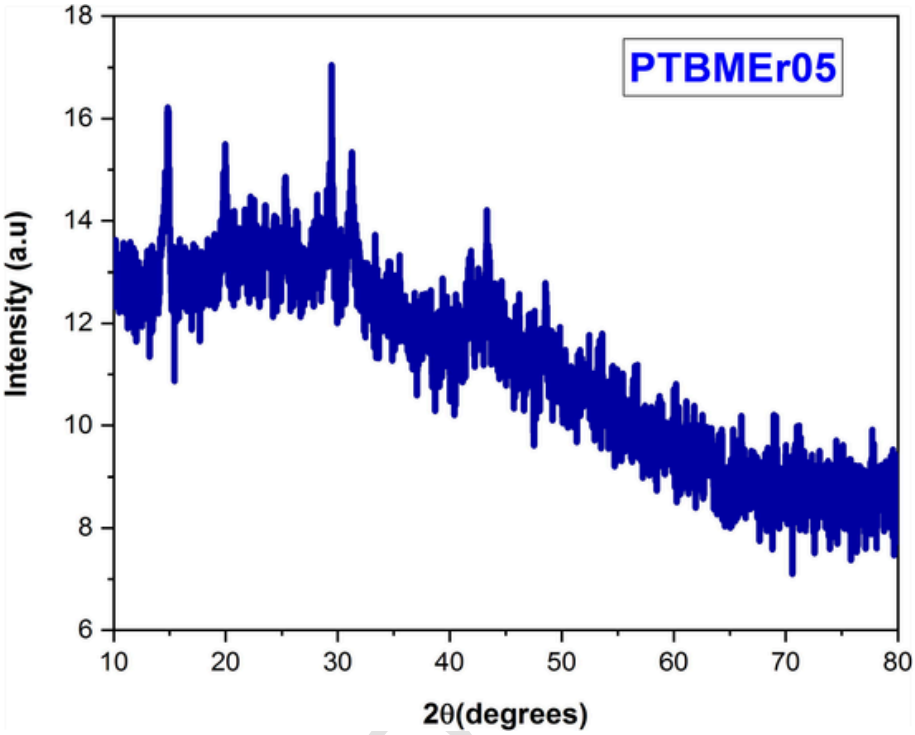

Fig. 2. XRD profile of PTBMEr05 glass.

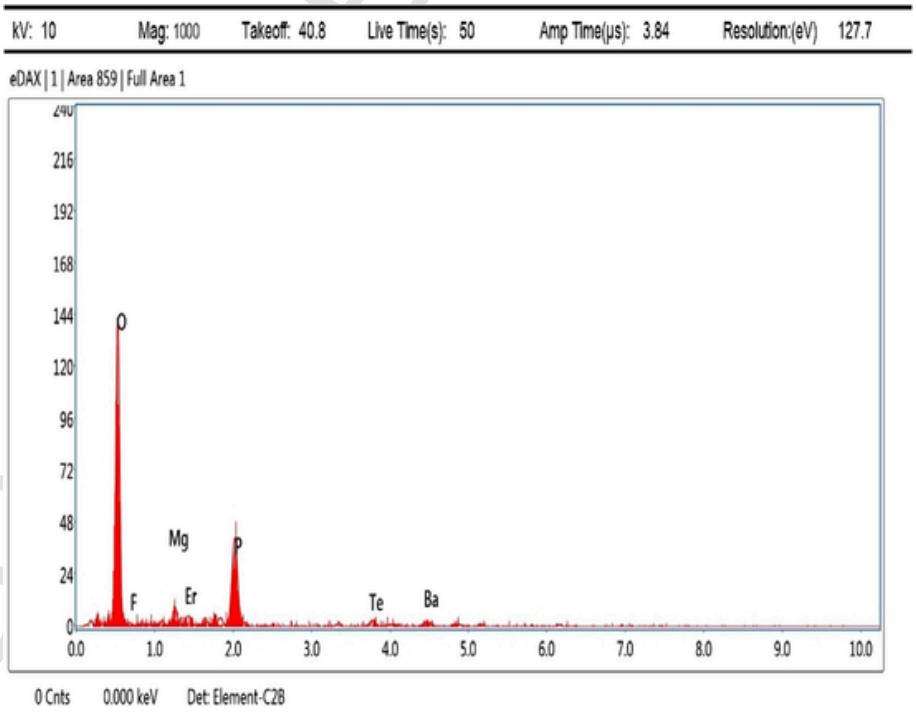

Fig. 3. EDX spectrum of PTBMEr05 glass.

3.2. *Structural analysis*

The XRD pattern forthe fabricated PTBMEr05 was documented and displayed in Fig. 2. The absence of clear peaks in the pattern serves as confirmation of the amorphous state of the prepared glasses [15,16]. In order to validate the elemental composition, an energy dispersive X-ray (EDX) spectrum was obtained for PTBMEr05 glass and is illustrated in Fig. 3. Table 2 provides the weight percentages of constituent elements and confirms the constituent elements of the glass composition. Fig. 4. demonstrates the Differential Scanning Calorimetry (DSC) curve specif-

Table 2
EDX measurements of element weights in PTBMEr05 glass.

Element	Weight %	Atomic %
O K	28.23	58.68
F K	0.09	0.16
Mg K	3.21	4.39
ErM	3.84	0.76
P K	24.13	25.91
TeL	15.17	3.95
BaL	25.33	6.14
Total	100	100

ically related to the PTBMEr05 sample. The graph reveals that the prepared sample exhibited thermal stability and rigidity, as evidenced by its thermal stability (ΔT) value of 152 ˚C.

Fig. 5. illustrates the FTIR spectra of PTBMEr glasses with complete band assignments. These spectra were acquired with a spectral resolution of 2 cm^{-1}, covering the range of 500–4000 cm^{-1}. The recording aimed to identify the specific groups. The tabulated Table 3 includes band positions and their corresponding assignments.

3.3. Optical absorption analysis

Fig. 6 (a), (b) depicts the absorption spectra of PTBMEr glasses, encompassing various concentrations of erbium ions. Significantly, there are 12 distinct bands that appear at wavelengths of 340, 360, 375, 403, 450, 484, 517, 541, 648, 798, 969, and 1528 nm. The peaks observed are caused by the electronic transitions of erbium from the ground state $^4I_{15/2}$ to the excited states $^2G_{7/2}$, $^4G_{9/2}$, $^4G_{11/2}$, $^2H_{9/2}$, $^4F_{5/2}$, $^4F_{7/2}$, $^2H_{11/2}$, $^4S_{3/2}$, $^4F_{9/2}$, $^4I_{9/2}$, $^4I_{11/2}$, and $^4I_{13/2}$ respectively [24]. Within these transitions, those from $^4I_{15/2}$ to $^4G_{11/2}$ and $^2H_{11/2}$ exhibit intense peaks, recognized as hypersensitive transitions. The selection criteria specified in the reference are followed by these transitions [13].

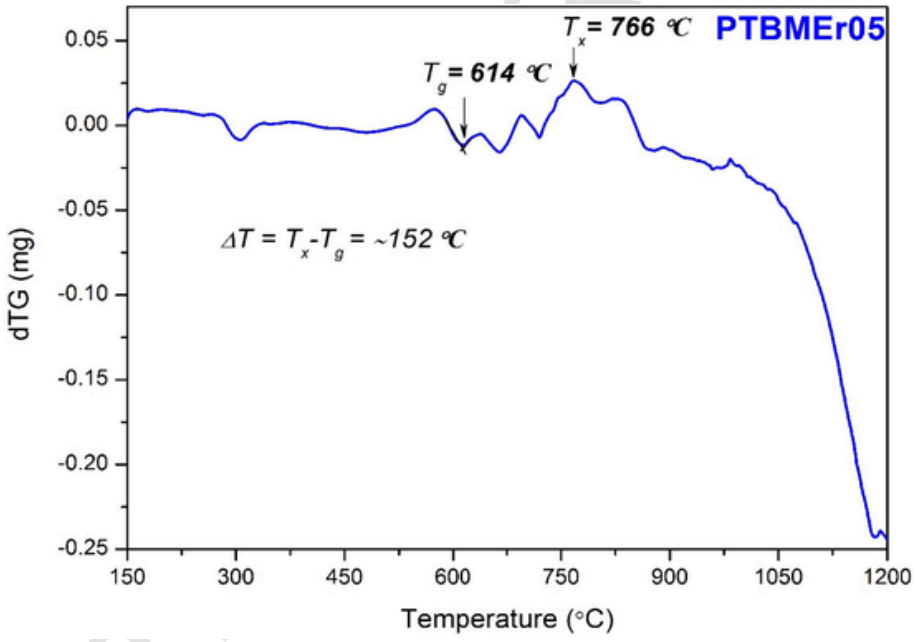

Fig. 4. DSC pattern of PTBMEr05 glass.

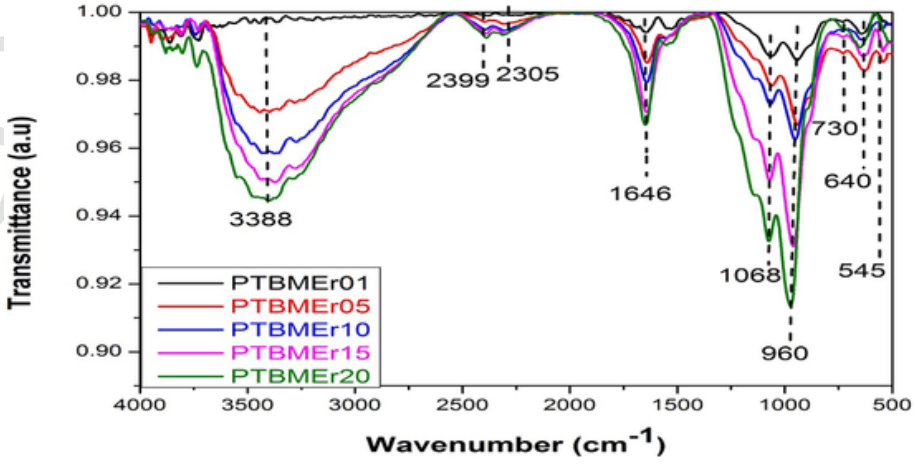

Fig.5. FTIR spectra of PTBMEr glasses.

Table 3
IR band assignments of PTBMEr glasses.

S.No	Band position (cm^{-1})	Band assignment	Reference
1	545	O-P-O units and PO_2 modes of (PO_3) Chains	[17]
2	640	Stretching modes of [TeO_4] trigonal bipyramidal units with the bridging oxygen	[18]
3	730	Symmetric stretching mode of P-O-P chains	[19,20]
4	960, 1086	Asymmetric stretching vibration of bridging oxygen atoms in P-O-P bonds and vibrations of diphosphate units (PO_3)	[21]
5	1646	P-O–H bridge	[22]
6	2305, 2399	P-O–H stretching vibrations	[22]
7	3388	Stretching of OH or water groups	[23]

Using the recorded optical absorption spectra, we computed experimental oscillatory strengths for diverse absorption transitions across all concentrations, employing the formulae outlined in the literature [25,26]. Employing Judd-Ofelt theory [27,28], oscillator strengths (f_{cal}) were evaluated and presented in Table 4, along with experimental oscillatory strengths (f_{exp}). By least-square fitting of experimental and calculated oscillator strengths, the Judd-Ofelt parameters (Ω_2, Ω_4, Ω_6) were determined [25]. The obtained J-O parameters were documented in Table 5 and compared with previous reports. The observed trend follows $\Omega_2 > \Omega_6 > \Omega_4$. The higher values of Ω_2 suggest an increased level of covalent bonding between O^{2-} ions and Er^{3+} ions [37]. In contrast, Ω_4 values are modest. The results indicate that it supports a decline in covalency in σ chemical bonds that exist among the ligand anions and rare earth ions. Furthermore, the value of Ω_6 is substantial, indicating a considerable level of inflexibility in the metal–ligand bond donation, specifically from some ligands possessing a tetrahedral structure such as PO_4 [31].

3.4. Photoluminescence

3.4.1. Visible photoluminescence

To explore various possibilities for achieving green luminescence, the excitation spectrum of PTBMEr05 glass was recorded within the spectral range of 350–500 nm. The emission at 1534 nm was moni-

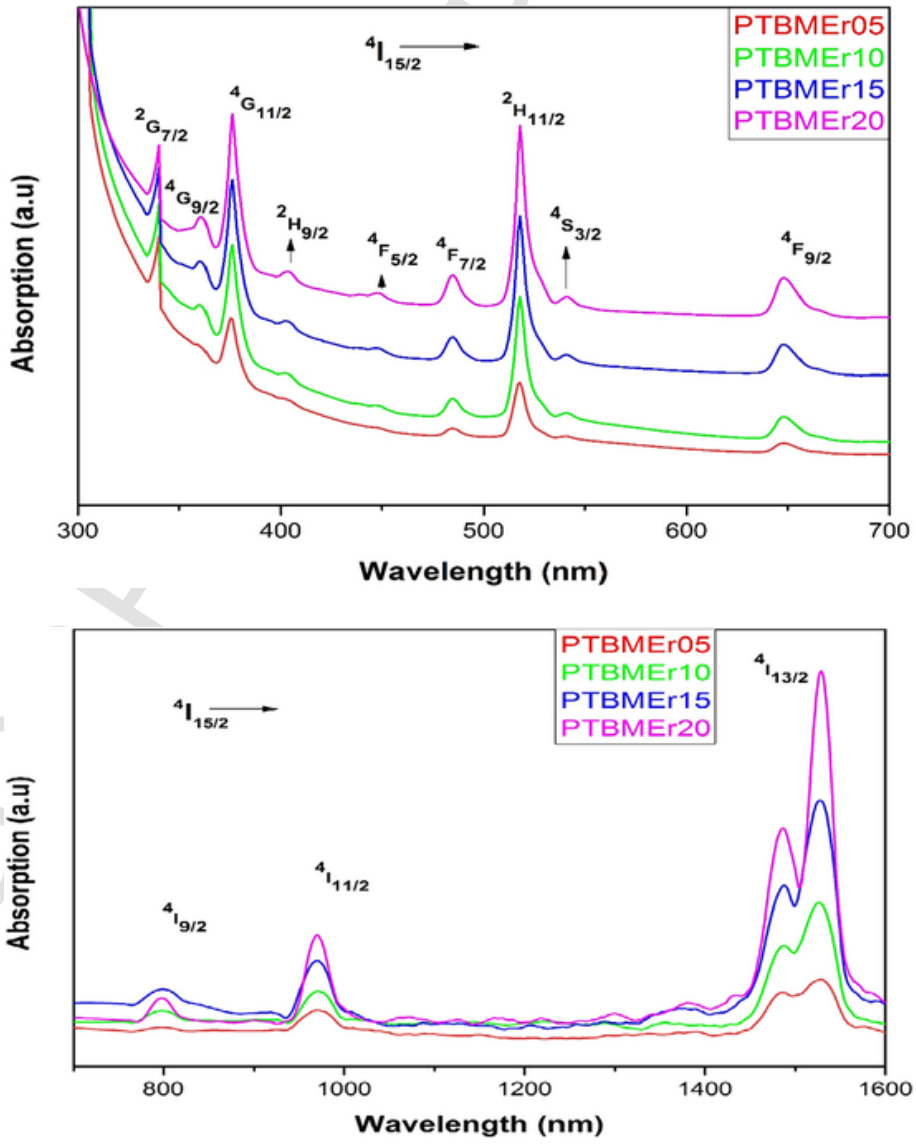

Fig. 6. (a) UV–Visible, (b) NIR absorption spectra of PTBMEr glasses.

Table 4
Experimental (f_{exp}) and calculated (f_{cal}) spectral intensities of erbium ions of various absorption bands in the PTBMEr glasses.

S.No	Absorption transition	Band positions		Oscillator strengths (x10^{-6})							
		Wavelength (nm)	Wavenumber (cm^{-1})	PTBMEr05		PTBMEr10		PTBMEr15		PTBMEr20	
				f_{exp}	f_{cal}	f_{exp}	f_{cal}	f_{exp}	f_{cal}	f_{exp}	f_{cal}
1	$^4I_{15/2} \rightarrow {}^2G_{7/2}$	340	29,411	1.172	0.898	1.325	1.117	1.772	0.761	1.091	0.890
2	$^4I_{15/2} \rightarrow {}^4G_{9/2}$	360	27,778	0.794	1.057	1.447	1.514	1.131	0.885	1.690	1.296
3	$^4I_{15/2} \rightarrow {}^4G_{11/2}$	375	26,667	18.163	18.155	33.741	33.423	17.725	17.709	10.601	10.775
4	$^4I_{15/2} \rightarrow {}^2H_{9/2}$	403	24,814	2.515	2.95	3.298	3.860	1.044	2.467	3.774	3.760
5	$^4I_{15/2} \rightarrow {}^4F_{5/2}$	450	22,222	1.359	1.07	0.762	0.701	0.621	0.862	0.785	0.850
6	$^4I_{15/2} \rightarrow {}^4F_{7/2}$	484	20,661	2.772	2.906	2.450	2.285	1.538	0.437	3.214	3.926
7	$^4I_{15/2} \rightarrow {}^2H_{11/2}$	517	19,342	10.546	10.310	18.925	18.986	9.985	10.048	6.111	6.119
8	$^4I_{15/2} \rightarrow {}^4S_{3/2}$	541	18,484	0.817	0.886	0.651	0.580	0.579	0.714	0.394	1.222
9	$^4I_{15/2} \rightarrow {}^4F_{9/2}$	648	15,432	2.219	1.845	2.081	2.290	1.934	1.534	1.700	0.235
10	$^4I_{15/2} \rightarrow {}^4I_{9/2}$	798	12,531	0.412	0.091	0.557	0.312	0.382	0.085	0.388	0.079
11	$^4I_{15/2} \rightarrow {}^4I_{11/2}$	969	10,319	1.439	1.073	0.933	0.932	1.166	0.900	1.396	1.318
12	$^4I_{15/2} \rightarrow {}^4I_{13/2}$	1528	6544	2.211	2.141	1.743	1.604	2.971	1.741	2.983	2.853
				δ_{rms} = 0.343		δ_{rms} = 0.239		δ_{rms} = 0.310		δ_{rms} = 0.671	

Table 5
Comparison of J-O parameters $\Omega_\lambda \times 10^{-20}$ cm^2 (λ = 2, 4 and 6) in various Er_2O_3 doped glasses with PTBMEr glass samples.

S.No	Glass host	Ω_2	Ω_4	Ω_6	Trend	Ref
1	PTBMEr05	7.039	0.363	2.181	$\Omega_2 > \Omega_6 > \Omega_4$	Present Work
2	PTBMEr10	12.805	1.423	1.520	$\Omega_2 > \Omega_6 > \Omega_4$	Present Work
3	PTBMEr15	6.135	0.865	1.859	$\Omega_2 > \Omega_6 > \Omega_4$	Present Work
4	PTBMEr20	0.653	0.018	0.320	$\Omega_2 > \Omega_6 > \Omega_4$	Present Work
5	PANBK1.5Er	0.43	0.31	0.39	$\Omega_2 > \Omega_6 > \Omega_4$	[29]
6	PPbKANEr10	4.79	0.78	1.22	$\Omega_2 > \Omega_6 > \Omega_4$	[30]
7	PB1	1.2944	0.0157	0.6990	$\Omega_2 > \Omega_6 > \Omega_4$	[31]
8	PB2	1.3810	0.0139	0.9704	$\Omega_2 > \Omega_6 > \Omega_4$	[31]
9	PB3	1.3471	0.0112	1.4000	$\Omega_2 > \Omega_6 > \Omega_4$	[31]
10	PB4	1.3208	0.0111	1.5544	$\Omega_2 > \Omega_6 > \Omega_4$	[31]
11	PKAPbNEr10	4.79	0.79	1.22	$\Omega_2 > \Omega_6 > \Omega_4$	[32]
12	$Li_2B_4O_7$:Er	12.07	2.40	3.87	$\Omega_2 > \Omega_6 > \Omega_4$	[33]
13	LBBPE01	13.609	1.098	2.610	$\Omega_2 > \Omega_6 > \Omega_4$	[34]
14	LBBPE03	11.339	1.178	2.729	$\Omega_2 > \Omega_6 > \Omega_4$	[34]
15	LBBPE05	8.734	2.243	2.700	$\Omega_2 > \Omega_6 > \Omega_4$	[34]
16	BaKAP	9.341	1.732	1.809	$\Omega_2 > \Omega_6 > \Omega_4$	[35]
17	LiZnLaAP	9.446	1.805	1.839	$\Omega_2 > \Omega_6 > \Omega_4$	[35]
18	LiMgLaAP	8.717	1.693	1.854	$\Omega_2 > \Omega_6 > \Omega_4$	[35]
19	LiZnLaAPF	11.74	2.030	2.250	$\Omega_2 > \Omega_6 > \Omega_4$	[35]
20	PKAZFEr05	7.11	0.97	2.37	$\Omega_2 > \Omega_6 > \Omega_4$	[36]
21	PKAZFEr10	8.23	1.04	1.91	$\Omega_2 > \Omega_6 > \Omega_4$	[36]

tored, and the obtained spectrum is presented in Fig. 7. The excitation peaks in the spectrum manifest at positions 357, 365, 377, 406, 443, 450, and 488 nm, corresponding to the transitions of erbium ions from the $^4I_{15/2}$ ground state to the $^2G_{7/2}$, $^4G_{9/2}$, $^4G_{11/2}$, $^2H_{9/2}$, $^4F_{3/2}$, $^4F_{5/2}$, and $^4F_{11/2}$ excited states respectively. According to the spectrum analysis, the excitation band with maximum intensity, centered at 377 nm, can be effectively used as the excitation wavelength [17].

Fig. 8. showcases the visible photoluminescence spectra of PTBMEr glasses, which were captured at 377 nm excitation and spanning the wavelength range of 450–700 nm. Remarkably, two distinguishable green emission bands are observable, with centers at 524 nm pertaining to the transition $^2H_{11/2} \rightarrow {}^4I_{15/2}$ and 544 nm pertaining to the transition $^4S_{3/2} \rightarrow {}^4I_{15/2}$. Further, there is an additional red emission band of low intensity, which is centered at 654 nm, pertaining to the transition $^4F_{9/2} \rightarrow {}^4I_{15/2}$ [17]. The radiative characteristics of PTBMEr glasses, including the radiative transition probabilities (A_R), radiative lifetimes (τ_{rad}), and branching ratios (β_R), were computed based on refractive index values and J-O parameter values. The formulae outlined in the literature [34] were employed to compute these parameters, which are detailed in Table 6. For PTBMEr05, PTBMEr10, PTBMEr15, and PTBMEr20, the stimulated emission cross section (σ_{emi}) values for the transition $^4S_{3/2} \rightarrow {}^4I_{15/2}$ are as follows: 0.75 × 10^{-20} cm^2, 0.45 × 10^{-20} cm^2, 0.59 × 10^{-20} cm^2, and 0.51 × 10^{-20} cm^2, respectively. Among the prepared samples, the PTBMEr05 sample demonstrates the greatest stimulated emission cross section value for the transition $^4S_{3/2} \rightarrow {}^4I_{15/2}$, signifying that it can be used as a viable contender for green laser emission devices [38].

3.4.2. NIR photoluminescence

Using an excitation wavelength of 980 nm, the synthesized sample's NIR photoluminescence spectra were acquired within the spectral range of 1450–1650 nm. Fig. 9. highlights the obtained spectra. It has been confirmed that there is a singular prominent emission band, centered at 1534 nm, pertaining to the transition $^4I_{13/2} \rightarrow {}^4I_{15/2}$. The slight shift of the luminescent peak towards the red region is attributed to reabsorption [39]. The radiative parameters for the transition $^4I_{13/2} \rightarrow {}^4I_{15/2}$, including radiative lifetime (τ_{rad}), radiative transition probability (A_R), effective bandwidth ($\Delta\lambda_{eff}$), stimulated emission cross section (σ_{emi}), optical gain ($\sigma_{emi} \times \tau_{rad}$), and gain bandwidth ($\sigma_{emi} \times \Delta\lambda_{eff}$), were assessed and outlined in Table 7. The analysis has revealed that the PTBMEr05 glass has been determined to possess an optimal optical gain value of 53.408 × 10^{-24} cm^2s and a gain bandwidth of 64.877 × 10^{-27} cm^3. This indicates that PTBMEr05 glass stands out as a prominent candidate for the amplification process at 1.53 μm.

3.5. Decay lifetime analysis

Fig. 10. illustrates the decay curves of excited state $^4I_{13/2}$ of erbium ions in PTBMEr glasses when excited at 980 nm. A uniform bi-exponential pattern is observed in the decay profiles of every sample. The experimental lifetimes for various concentrations were determined using a formula available in the literature [40] and are presented in Table 8. The reduction in experimental lifetime as the concentration increases can be attributed to the presence of quenching centers and the heightened non-radiative energy migration between erbium ions [45].

4. Conclusions

Erbium-doped Oxyfluoro telluro phosphate glasses were synthesized, and a comprehensive examination was conducted to analyse their structural, optical, and luminescent characteristics. the XRD study reported that the synthesized samples were amorphous, and FTIR analysis identified the presence of various structural units of tellurite and phosphate. The optical absorption spectra were used to assess Judd-Oflet (J-O) parameters and radiative parameters. A higher value of Ω_2 reports a decline in the covalency of the σ chemical bonds that exist among ligand anions and the rare earth ions. The emission spectra

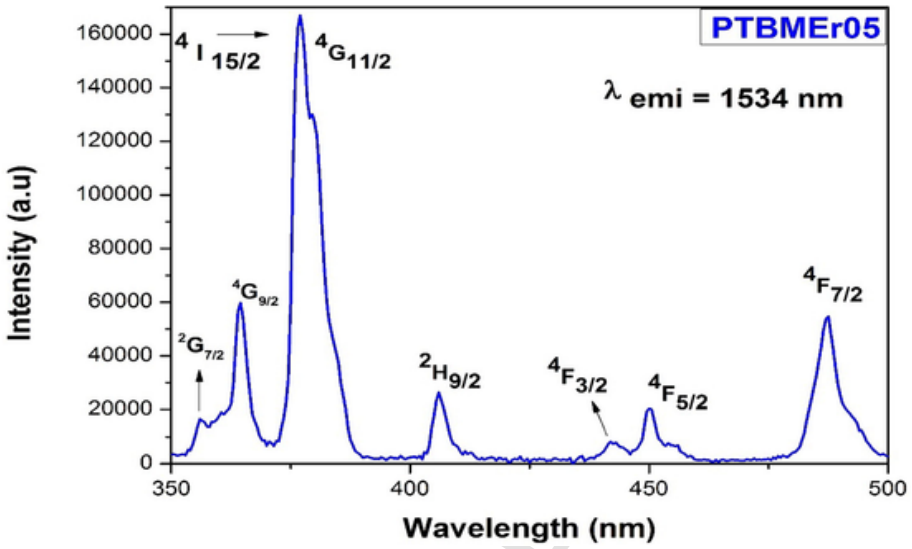

Fig. 7. Excitation spectrum of PTBMEr05 glass.

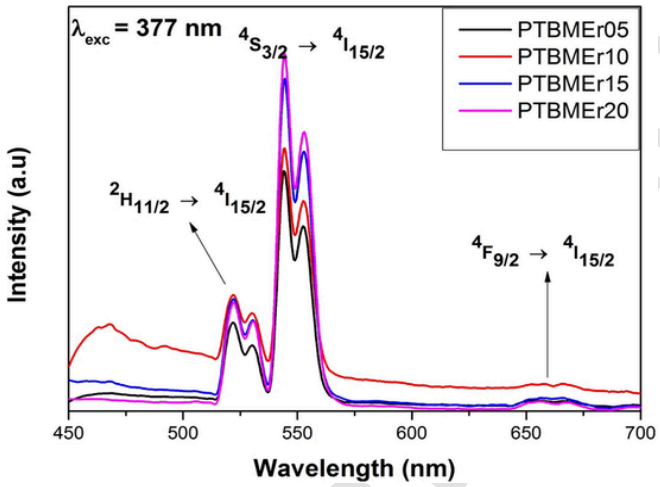

Fig. 8. Visible emission spectra of PTBMEr glasses.

revealed a pronounced green emission band ($^4S_{3/2}\rightarrow{}^4I_{15/2}$) and a strong near-infrared (NIR) emission band ($^4I_{13/2}\rightarrow{}^4I_{15/2}$). Under 980 nm excitation, decay analysis was carried out for level $^4I_{13/2}$. It is observed that the experimental lifetime value decreases with a rise in concentration. Within the prepared samples, the PTBMEr05 sample stands out with higher metrics, showcasing a gain bandwidth of 64.87 × 10^{-25} cm^3, a stimulated emission cross section of 0.75 × 10^{-20} cm^2 for $^4S_{3/2}\rightarrow{}^4I_{15/2}$ and 1.19 × 10^{-20} cm^2 for $^4I_{13/2}\rightarrow{}^4I_{15/2}$, and an optical gain of 53.41 × 10^{-24} cm^2S. These results reflect that PTBMEr05 glass is best suited for green laser emission devices and optical fiber communication windows.

Declaration of competing interest

The authors declare that they have no known competing financial interests or personal relationships that could have appeared to influence the work reported in this paper.

Data availability

Data will be made available on request.

Table 6
Emission transitions (SLJ → S'L'J'), energy gap (ΔE, cm^{-1}), radiative transition probability (A_R, s^{-1}), branching ratios (β_R), and radiative life times (τ_R, ms) of PTBMEr glasses.

	Initial state SLJ	**Final state** S'L'J'	ΔE	A_R	β_R	τ_R
For PTBMEr05	$^4S_{3/2}$	$^4F_{9/2}$	3057	1.06	0.0003	
		$^4I_{9/2}$	5934	83.32	0.0265	
		$^4I_{11/2}$	8187	65.66	0.0209	
		$^4I_{13/2}$	11,936	871.57	0.2770	
		$^4I_{15/2}$	18,480	2124.99	0.6753	317
	$^4F_{9/2}$	$^4I_{9/2}$	2877	9.11	0.0064	
		$^4I_{11/2}$	5130	128.63	0.0909	
		$^4I_{13/2}$	8879	59.03	0.0417	
		$^4I_{15/2}$	15,423	1218.05	0.8609	706
	$^4I_{9/2}$	$^4I_{11/2}$	2253	2.48	0.0181	
		$^4I_{13/2}$	6002	92.96	0.6763	
		$^4I_{15/2}$	12,546	42.02	0.3057	7274
	$^4I_{11/2}$	$^4I_{13/2}$	3749	42.44	0.1377	
		$^4I_{15/2}$	10,293	265.87	0.8623	3243
	$^4I_{13/2}$	$^4I_{15/2}$	6544	222.79	1.0000	4488
For PTBMEr10	$^4S_{3/2}$	$^4F_{9/2}$	3006	0.71	0.0003	
		$^4I_{9/2}$	5916	70.43	0.0319	
		$^4I_{11/2}$	8162	47.82	0.0217	
		$^4I_{13/2}$	11,893	604.53	0.2743	
		$^4I_{15/2}$	18,442	1480.80	0.6718	453
	$^4F_{9/2}$	$^4I_{9/2}$	2910	4.57	0.0027	
		$^4I_{11/2}$	5156	84.43	0.0506	
		$^4I_{13/2}$	8887	68.71	0.0412	
		$^4I_{15/2}$	15,436	1509.38	0.9054	599
	$^4I_{9/2}$	$^4I_{11/2}$	2246	2.36	0.0117	
		$^4I_{13/2}$	5977	64.95	0.3221	
		$^4I_{15/2}$	12,526	134.35	0.6662	5178
	$^4I_{11/2}$	$^4I_{13/2}$	3731	33.37	0.1728	
		$^4I_{15/2}$	10,280	159.73	0.8272	5178
	$^4I_{13/2}$	$^4I_{15/2}$	6549	172.99	1.0000	5780
	Initial state SLJ	**Final state** S'L'J'	ΔE	A_R	β_R	τ_R
For PTBMEr15	$^4S_{3/2}$	$^4F_{9/2}$	3056	0.91	0.0003	
		$^4I_{9/2}$	5973	79.15	0.0292	
		$^4I_{11/2}$	8161	56.93	0.0210	
		$^4I_{13/2}$	11,936	748.98	0.2761	
		$^4I_{15/2}$	18,481	1826.41	0.6734	368
	$^4F_{9/2}$	$^4I_{9/2}$	2917	8.77	0.0057	
		$^4I_{11/2}$	5105	110.56	0.0716	
		$^4I_{13/2}$	8880	67.54	0.0438	
		$^4I_{15/2}$	15,425	1356.64	0.8789	647
	$^4I_{9/2}$	$^4I_{11/2}$	2188	2.25	0.0135	
		$^4I_{13/2}$	5963	78.65	0.4728	
		$^4I_{15/2}$	12,508	85.44	0.5136	6011
	$^4I_{11/2}$	$^4I_{13/2}$	375	40.02	0.1475	
		$^4I_{15/2}$	10,320	231.30	0.8525	3685
	$^4I_{13/2}$	$^4I_{15/2}$	6545	201.47	1.0000	4963

Table 6 (*continued*)

	Initial state SLJ	**Final state** S'L'J'	ΔE	A_R	β_R	τ_R
For PTBMEr20	$^4S_{3/2}$	$^4F_{9/2}$	3061	0.83	0.0003	
		$^4I_{9/2}$	5978	65.04	0.0264	
		$^4I_{11/2}$	8180	50.90	0.0207	
		$^4I_{13/2}$	11,954	683.75	0.2775	
		$^4I_{15/2}$	18,495	1663.60	0.6751	405
	$^4F_{9/2}$	$^4I_{9/2}$	2917	5.39	0.0053	
		$^4I_{11/2}$	5119	92.80	0.0917	
		$^4I_{13/2}$	8893	35.45	0.0350	
		$^4I_{15/2}$	15,434	878.40	0.8680	988
	$^4I_{9/2}$	$^4I_{11/2}$	2202	2.06	0.0219	
		$^4I_{13/2}$	5976	71.51	0.7596	
		$^4I_{15/2}$	12,517	20.57	0.2185	1062
	$^4I_{11/2}$	$^4I_{13/2}$	3774	34.61	0.1573	
		$^4I_{15/2}$	10,315	185.37	0.8427	4545
	$^4I_{13/2}$	$^4I_{15/2}$	6541	178.99	1.0000	5586

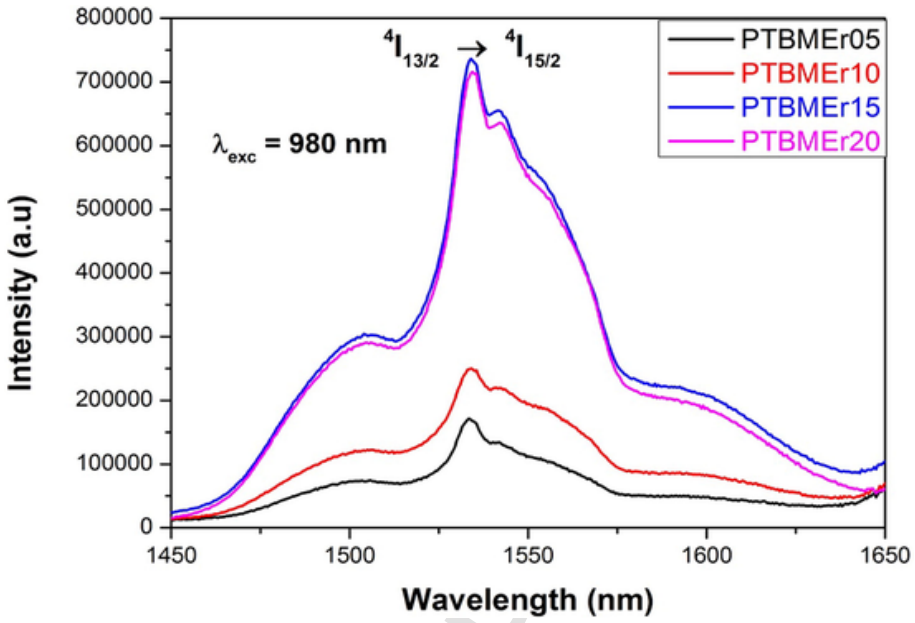

Fig. 9. NIR emission spectra of PTBMEr glasses.

Table 7
Comparison of radiative properties of the transition $^4I_{13/2} \rightarrow {}^4I_{15/2}$ of Er^{3+} ions doped glasses with previously reported glasses.

S.No	Glass sample	λ_p(nm)	A_R (s^{-1})	τ_{rad} (ms)	$\Delta\lambda_{eff}$ (nm)	σ_{emi} ($\times 10^{-20} cm^2$)	$\sigma_{emi} \times \Delta\lambda_{eff}$ ($\times 10^{-27}$ cm^3)	$\sigma_{emi} \times \tau_{rad}$ ($\times 10^{-24}$ $cm^2 s$)	Ref
1	PTBMEr05	1535.5	222.79	4.488	54.51	1.19	64.87	53.41	[present work]
2	PTBMEr10	1534	172.99	5.780	61.04	0.83	50.66	47.97	[present work]
3	PTBMEr15	1534	201.47	4.963	62.07	0.95	58.97	47.15	[present work]
4	PTBMEr20	1534.5	178.99	5.586	61.10	0.85	51.93	47.75	[present work]
5	$PBaLaEr_{1.0}$	1534	270.41	3.69	59	1.36	80.12	50.11	[17]
6	PNAEr7.0	1531	–	9.160	57	0.548	27.27	44.6	[30]
7	PNAEr8.0	1531	–	10.280	56	0.487	27.272	50.06	[30]
8	SALSFEr10	1530	250.4	3.99	63	1.16	73.08	46.28	[38]
9	OCBTEr1.0	1536	215.78	4.634	55.40	0.564	31.25	26.13	[41]
10	PKAZFEr10	1535	177.18	5.64	31	0.519	16.09	29.27	[42]
11	PBEr0.5	1531	151.26	4.48	26	0.99	25.74	44.35	[43]
12	PBEr1.0	1531	136.61	3.50	26.8	0.89	23.85	31.15	[43]
13	PBEr1.5	1531	217.16	1.52	31.9	1.56	49.76	23.71	[43]
14	EDLP1	1530	246.63	2.75	27	0.845	22.81	23.23	[44]
15	EDLP2	1530	–	1.48	32	0.845	27.04	12.50	[44]
16	EDLP3	1530	–	0.85	33.5	0.845	28.31	12.51	[44]
17	EDLP4	1530	–	0.63	40	0.845	33.80	5.32	[44]

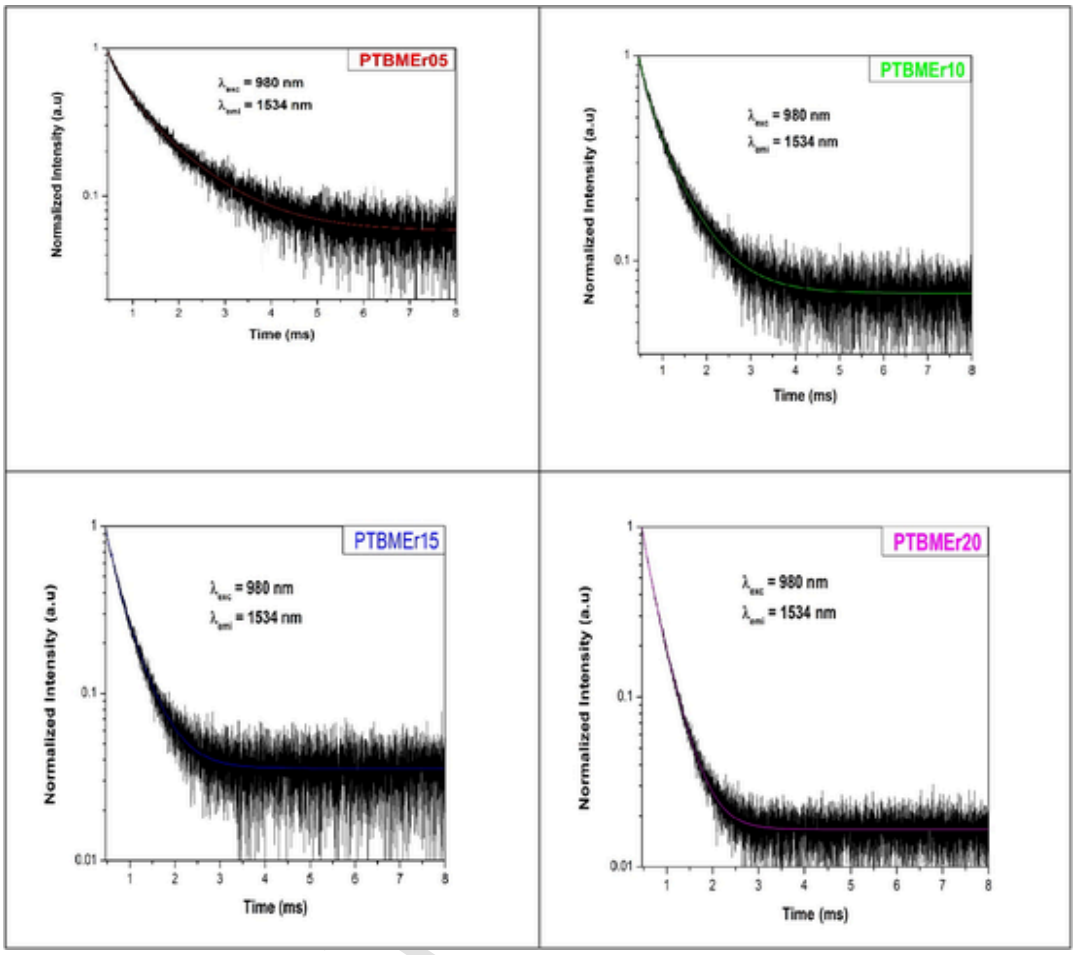

Fig. 10. Photoluminescence decay curves of $^4I_{13/2}$ to $^4I_{15/2}$ transition under 980 nm laser excitation of PTBMEr glasses.

Table 8
Comparison of fluorescent lifetime of $^4I_{13/2}$ excited level of Er^{3+} ions in PTBMEr glasses with other glasses doped with erbium.

S.No	Sample	τ_{exp}(ms)	Ref
1	PTBMEr05	1.0556	Present Work
2	PTBMEr10	1.1009	Present Work
3	PTBMEr15	0.4385	Present Work
4	PTBMEr20	0.3414	Present Work
5	$PBaLaEr_{1.0}$	1.283	[17]
6	PPbKANEr2.0	1.26	[30]
7	PPbKANEr4.0	0.62	[30]
8	PPbKANEr1.0	1.69	[30]
9	$Li_2B_4O_7$:Er0.5	0.390	[33]
10	$Li_2B_4O_7$:Er1.0	0.393	[33]
11	LBBPE01	1.04	[34]
12	LBBPE03	1.01	[34]
13	LBBPE05	0.90	[34]
14	PCfBfTiEr0.1	2.11	[39]
15	PCfBfTiEr0.5	0.91	[39]

References

[1] Wojciech A. Pisarski, Karolina Kowalska, Marta Kuwik, Joanna Pisarska, Dominik DoroszMarcin Kochanowicz, Jacek˙Zmojda, Jan Dorosz Enhanced mid-IR luminescence of Er^{3+} ions at 2.7 μm in TiO_2-GeO_2-BaO-Ga_2O_3 glasses, J. Lumin. 265 (2024) 120227, DOI: 10.1016/j.jlumin.2023.120227.

[2] S. Jackson, R. Vallee, M. Bernier, Mid-Infrared Fiber Photonics: Glass Materials, Fiber Fabrication and Processing, Laser and Nonlinear Sources, Woodhead Publishing (2021), https://doi.org/10.1016/B978-0-12-818017-4.10000-X.

[3] J. Hu, L. Mawst, S. Moss, L. Petit, D. Ting, Feature issue introduction: mid-infrared optical materials and their device applications, Opt. Mater. Express 8, 2026–2034, Opt. Mater. Express (2018), https://doi.org/10.1364/OME.8.002026.

[4] S.D. Jackson, R.K. Jain, Fiber-based sources of coherent MIR radiation: key advances and future prospects (invited), Opt. Express 28 (2020) 30964–31019, https://doi.org/10.1364/OE.400003.

[5] H. Es-souf, L. Bih, B. Manoun, P. Lazor, Structure, thermal analysis and optical properties of lithiumtungsten-titanophosphate glasses, J. Non-Cryst. Solids 463 (2017) 12–18, https://doi.org/10.1016/j.jnoncrysol.2017.02.013.

[6] B.C. Sales, L.A. Boatner, Physical and chemical characteristics of lead-iron phosphate nuclear waste glasses, J. Non-Cryst. Solids. 79 (1986) 83–116, https://doi.org/10.1016/0022-3093(86)90040-2.

[7] Y.B. Peng, D.E. Day, High thermal expansion phosphate glasses. Part-1, Glass Technol. 32 (1991) 166, ISSN 0017-1050,

[8] G. Fuxi, New glass-forming systems and their practical application, J. Non-Cryst. Solids. 123 (1990) 385–399, https://doi.org/10.1016/0022-3093(90)90811-Y.

[9] N.V. Nikonorov, G.T. Petrovskii, Ion-exchanged glasses in integrated optics: The current state of research and prospects (a review), ISSN: 1087-6596eISSN: 1608-313X,

[10] J.A. Wilder, glasses and glass ceramics for sealing to aluminium alloys, J. Non-Cryst. Solids 38 (1980) 879, https://doi.org/10.1016/2200-3093(80)90548-7.

[11] D.K. Durga, P. Yadagiri Reddy, N. Veeraiah, Optical absorption and thermo luminescence properties of ZnF_2-MO-TeO_2 (M= As_2O_3, Bi_2O_3 and P_2O_5) glasses doped with chromium ions, J. Lumin. 99(2002) 53-60, DOI: 10.1016/S0022-2313(02)00293-4.

[12] K. Linganna, D. Viswanath, R. Narro Garcia, S. Ju, W. T. Han, C.K. Jayasankar, V. Venkatramu, Thermal and optical properties of Nd^{3+} ions K-Ca-Al fluorophosphate glasses, J. Lumin. 166(2015)328-334, http://dx.doi.org://10.1016/j.jlumni.2015.05.024.

[13] K. Selvaraj, K. Marimuthu, Structural and spectroscopic studies on concentration dependent Er3+ doped boro-tellurite glasses, J. Lumin. 132 (2012) 1171–1178, https://doi.org/10.1016/j.jlumin.2011.12.056.

[14] M.S Sajna, Sunil Thomas, K.A. Ann Mary, Cyriac Joseph, P.R. Biju, N. Unnikrishnan, Spectroscopic properties of Er^{3+} ions in multicomponent tellurite glasses, J. Lumin. 159(2015) 55-65, DOI: 10.1016/j.jlumin.2014.10.062.

[15] P. Goyal, Yogesh Kumar Sharma, Sudha Pal, Umesh Chandra Bind, Shu-Chi Huang, Shyan- Lung Chung, the effect of SiO2 content on structural, physical and

spectroscopic properties of Er3+ doped B2O3-SiO2-Na2O-PbO-ZnO glass systems, J. Non-Cryst. Solids. 463 (2017) 118–127, https://doi.org/10.1016/j.jnoncrysol.2017.03.009.
[16] G. Lifante, Martinez de medieval, R.He, E.Cantelar, L.Ortega San Martin, D.Sola, Transition probabilities of Er^{3+} ions in alumina-silicate glasses, J. Lumin. 203 (2018) 305-312, DOI: j.jlumin.2018.06.063.
[17] Pikkili Ramprasad, Ch. Basavapoornima, C. R. Kesavulu, Venkatramu, J. Kaewkhao, C.K. Jayasankar, Spectroscopic properties of Er^{3+} - doped barium phosphate glasses for optical gain media, Results Opt. 12(2023) 100489, DOI: 10.1016/j.rio.2023.100489.
[18] S. Rada, Eu gen Culea, FTIR spectroscopic and DFT theoretical study on structure of europium-phosphate-tellurite glasses and glass ceramics, J. Mol. Struct. 929 (2009) 141–148, https://doi.org/10.1016/j.molstruc.2009.04.021.
[19] M. De, S. Jana, Subrata Mitra, Structural and spectroscopic characteristics of Eu3+ embedded titanium lead phosphate glasses for red luminescence, Solid State Sci. 114 (2021) 106560, https://doi.org/10.1016/j.solidstatesciences.2021.106560.
[20] V. Sudarshan, R. Mishra, S.K. Kulshreshtha, Thermal and structural studies on TeO2 substituted (PbO)0.5(P2O5)0.5 glasses, J. Non-Cryst. Solids. 342 (2004) 160–165, https://doi.org/10.1016/j.jnoncrysol.2004.07.014.
[21] P. Mosner, K. Vosejpkova, L. Koudelka, L. Montagne, B. Revel, Structure and properties of ZnO-B_2O_3-P_2O_5-TeO_2 glasses, Mater. Chem. Phys. 124 (2010) 732–737, https://doi.org/10.1026/j.matchemphys.20101.07.048.
[22] V.N. Rai, B.N. Raja Sekhar, D.M. Phase, S.K. Deb, Effect of gamma irradiation on the structure and valence state of Nd in phosphate glass, Mater. Sci. DOI: 10.48550/arXiv.1406.4686.
[23] S. Selvi, K. Marimuthu, G. Muralidharan, Effect of PbO on the B_2O_3-TeO_2-P_2O_5-BaO-CdO-Sm_2O_3 glasses- Structural and optical investigations, J. Non-Cryst. Solids. 461 (2017) 35–46, https://doi.org/10.1016/j.jnoncrysol.2017.01.028.
[24] Weiwei Ma, Liangbi Su, Xuedong Xu, Gingya Wang, Dapeng Jiang, Lihe Zheng, Xiuwei Fan, Chun Li, Jie Liu, Jun Xu, Effect of erbium concentration on spectroscopic properties and 2.79 μm laser performance of Er: CaF_2 crystals, Opt. Mater. Express. 409, https://doi:10.1364/OME.6.000409.
[25] Markus P. Hehlen, Mikhail G. Brik, Karl Kramer, 50^{th} anniversary of the Judd-Ofelt theory: An experimentalist's view of the formalism and its application. J. Lumin. 136, 221-239. DOI: 10.1016/j.jlumin.2012.10.035.
[26] Probabilities for Radiative and Nonradiative Decay of Er^{3+} in LaF_3, Weber M.J, Phys. Rev. 157(2), 262-272. DOI: 10.1103/physrev.157.262.
[27] B.R. Judd, Optical Absorption Intensities of Rare- Earth ions, Phys. Rev. 127 (3) (1962) 750–761, https://doi.org/10.1103/PhysRev.127.750.
[28] G.S. Oflet, Intensities of Crystal Spectra of Rare- Earth Ions, J. Chem. Phys. 37 (1962) 511, https://doi.org/10.1063/1.1701366.
[29] Mahmoud Mohammed Isamil, Hazem Farouk, Mohamed Ali Salem, Adel Ashery, Inas Kamal Battisha, Optical properties of Er^{3+} doped phosphate glasses, J.Sci. Res. Sci., Vol (36), 2019. DOI: 10.21608/jsrs.2019.58543.
[30] T. Maheswari, Ch. Basavapoornima, K. Linganna, S. Ju, W.T. Han, C.K. Jayasankar, Structural and spectroscopic properties of γ-ray irradiated Er3+ - doped lead phosphate glasses, J. Lumin 203 (2018) 322–330, https://doi.org/10.1016/j.jallcom.2016.12.199.
[31] N. Sdiri, H. Elhouichet, M. Ferid, Effects of substituting P_2O_5 for B_2O_3 on the thermal and optical properties of sodium borophosphate glasses doped with $Er^{3}+$, J. Non-Cryst. Solids. 389 (2014) 38–45, https://doi.org/10.1016/j.jnoncrysol.2014.01.031.
[32] Ch. Basavapoornima, K. Linganna, S. Ju, B.H. Kim, W.T. Han, C.K. Jayasankar, Spectroscopic and pump power dependent upconversion studies of Er3+ -doped lead phosphate glasses for photonic applications, J. Alloys Compd. (2017), https://doi.org/10.1016/j.jallcom.2016.12.199.
[33] B. V. Padlyak, R. Lisiecki, W. Ryba-Romanowski, Spectroscopy of the Er^{3+}-doped lithium tetra borate glasses, Opt.Mater. 54 (2016) 126-113, DOI: 10.1016/j.optmat.2016.02.025.
[34] A. Madhu, B. Eraiah, P. Manasa, Ch. Basavapoornima, Er^{3+} ions doped lithium-bismuth-boro-phosphate glass for 1532 nm emission and efficient red emission up conversion for telecommunication and lasing applications, J. Non-Cryst. Solids. 495 (2018) 35-46, DOI: 10/1016/j.jnoncrysol.2018.04.060.
[35] R. Lachheb, A. Herrmann, A.A. Assadi, K. Damak, C. Russel, R. Maalej, Judd Ofelt analysis and experimental spectroscopic study of erbium doped phosphate glasses, J. Lumin. (2018), https://doi.org/10.1016/j.jlumin.2018.03.087.
[36] V. B. Sreedhar, N. Vijaya, D. Ramachari, C. K. Jayasankar, Luminescence studies of Er^{3+}-doped zincfluorophosphate glasses for 1.53 μm laser applications, J. Mol. Struct., DOI: 10.1016/j.molstruc.2016.10.062.
[37] D. Gelija, L. Kadathala, D.P.R. Borelli, Energy transfer dynamics of Er3+/Nd3+ embedded SiO2-Al2O3-Na2CO3-SrF2-CaF2 glasses for optical communications, Opt. Mater. 78 (2018) 172–180, https://doi.org/10.1016/j.optmat.2018.02.021.
[38] C.R. Kesavulu, V.B. Sreedhar, C.K. Jayasankar, Kiwan Jang, Dong-Soo Shin, Soung Soo Yi, Structural, thermal and spectroscopic properties of highly Er3+ doped novel oxyfluoride glasses for photonic application, Mater. Res. Bull. 51 (2014) 336–344, https://doi.org/10.1016/j.materresbull.2013.12.023.
[39] Venkata Krishnaiah Kummara, Neelima G. , Ravi N. , Nanda Kumar Reddy Nallabala, Satish Kumar Reddy H. , Dwaraka Viswanath C.S, Lenine D, Surekha G. , Padma Suvarna R. , Yuwaraj C. , Venkatramu V. , Near infrared broadband and visible upconversion emissions of erbium ions in oxyfluoride glasses for optical amplifier applications, Opt. Laser Technol. 127 (2020) 106167, DOI: 10.1016/optlastec.2020.106167.
[40] N. Prasad, P. Reddi Babu, P. Pavithra, P. Chandra Sekhar, B. Deva Prasad Raju, J. Kaewkho, Optical and luminescence studies of Nd^{3+} doped phosphate Glasses for pulsed laser applications, Mater. Today: Proc., DOI: 10.1016/j.matpc.2023.05.179.
[41] R.A.A. Silva, N.F. Dantas, R.F. Muniz, A.M.O. Lima, F. Pedrochi, A. Steimacher, M.J. Barboz, Optical and spectroscopic properties of Er3+/Yb3+ co-doped calcium borotellurite glasses, J. Lumin. 251 (2022) 119239, https://doi.org/10.1016/j.jlumin.2022.119239.
[42] V.B. Sreedhar, N. Vijaya, D. Ramachari, C. K. Jayasankar, Luminescence properties of Er^{3+}-doped zincfluorophosphate glasses for 1.53 μm laser applications, J. Mol. Struct. S0022-2860(16) 3119-X, DOI: 10.1016/j.molstruc.2016.10.062.
[43] S. Hraiech, C. Bouzidi, M. Ferid, Luminescence properties of Er^{3+}-doped phosphate glasses, Phys. B: Condens. Matter S0921-4526(17)30445-3, DOI: 10.1016/j.physb.2017.07.047.
[44] C.C. Santos, I. Guedes, C.-K. Loong, L.A. Boatner, A.L. Moura, M.T. de Araujo, C. Jacinto, M.V.D. Vermelho, Spectroscopic properties of Er3+- doped lead phosphate glasses for photonic application, J. Phys. d: Appl. Phys. 43 (2010) 025102, https://doi.org/10.1088/0022-3727/43/2/025102.
[45] S.K. Taherunnisa, D.V. Krishna Reddy, T. Sambasiva Rao, K.S. Rudramamba, Y.A. Zhydachevskyy, A. Suchochi, M. Piasecki, M. Rami Reddy, Effect of up-conversion luminescence in Er^{3+} doped phosphate glasses for developing Erbium-Doped Fibre Amplifiers (EDFA) and G-LED's, Opt. Mater. DOI: 10.1016/j.omx.2019.100034.